

# Optical-parametric-amplification imaging of complex objects

Peter M. Vaughan<sup>1,\*</sup> and Rick Trebino<sup>1</sup>

<sup>1</sup>Georgia Institute of Technology, School of Physics 837 State Street, Atlanta, Georgia 30332, USA

\*petermvaughan@gatech.edu

**Abstract:** We used ultrafast Fourier-plane optical-parametric-amplification (OPA) imaging to simultaneously image, wavelength-shift, and amplify complex two-dimensional objects with spatial features from 1.1 to 10.1 line pairs/millimeter (lp/mm) in the vertical dimension and from 2.0 to 16.0 lp/mm in the horizontal dimension, corresponding to a two-dimensional space-bandwidth product (SBP) of  $\sim 46,000$ . This represents an increase in image complexity over previous analogous OPA imaging systems by over three orders of magnitude. We observe both wavelength-shifting the image from 930nm to a wavelength of 700nm and image amplification by two orders of magnitude. Our wavelength-shifted image has a SBP of  $\sim 30,000$ .

©2011 Optical Society of America

**OCIS codes:** (320.0320) Ultrafast optics; (320.7110) Ultrafast nonlinear optics; (190.7220) Up-conversion; (190.4970) Parametric oscillators and amplifiers; (110.3080) Infrared imaging.

---

## References and links

1. J. A. Armstrong, N. Bloembergen, J. Ducuing, and P. S. Pershan, "Interactions between light waves in a nonlinear dielectric," *Phys. Rev.* **127**(6), 1918–1939 (1962).
2. C. C. Wang and G. W. Racette, "Measurement of parametric gain accompanying optical difference frequency generation," *Appl. Phys. Lett.* **6**(8), 169–171 (1965).
3. F. Zernike and J. E. Midwinter, *Applied Nonlinear Optics* (Wiley, 1973).
4. J. E. Midwinter, "Image conversion from 1.6 $\mu$ m to the visible in lithium niobate," *Appl. Phys. Lett.* **12**(3), 68–71 (1968).
5. E. Lantz and F. Devaux, "Parametric amplification of images," *J. Opt. B Quantum Semiclassical Opt.* **9**(2), 279–286 (1997).
6. F. Devaux and E. Lantz, "Parametric amplification of a polychromatic image," *J. Opt. Soc. Am. B* **12**(11), 2245–2253 (1995).
7. F. Devaux, E. Lantz, A. Lacourt, D. Gindre, H. Maillotte, P. A. Doreau, and T. Laurent, "Picosecond parametric amplification of a monochromatic image," *Nonlinear Opt.* **11**, 25–38 (1995).
8. F. Devaux and E. Lantz, "Transfer function of spatial frequencies in parametric image amplification: experimental analysis and application to picosecond spatial filtering," *Opt. Commun.* **114**(3-4), 295–300 (1995).
9. J. Goodman, *Introduction to Fourier Optics* (Roberts & Company Publishers, 2004).
10. D. Guthals and D. Sox, "Quantum limited optical parametric image amplification," in *Proceedings of the International Conference on Lasers*, 1989), 808–816.
11. G. W. Faris and M. Banks, "Upconverting time gate for imaging through highly scattering media," *Opt. Lett.* **19**(22), 1813–1816 (1994).
12. A. H. Firester, "Image upconversion: part III," *J. Appl. Phys.* **41**(2), 703–710 (1970).
13. P. V. Avizonis, F. A. Hopf, D. W. Bomberger, S. F. Jacobs, A. Tomita, and K. H. Womack, "Optical phase conjugation in a lithium formate crystal," *Appl. Phys. Lett.* **31**(7), 435–438 (1977).
14. L. Lefort and A. Barthelemy, "Revisiting optical phase conjugation by difference-frequency generation," *Opt. Lett.* **21**(12), 848–850 (1996).
15. F. Devaux, G. Le Tolguenec, and E. Lantz, "Phase conjugate imaging by type II parametric amplification," *Opt. Commun.* **147**(4-6), 309–312 (1998).
16. A. W. Lohmann, R. G. Dorsch, D. Mendlovic, Z. Zalevsky, and C. Ferreira, "Space-bandwidth product of optical signals and systems," *J. Opt. Soc. Am. A* **13**(3), 470–473 (1996).
17. F. Devaux, A. Mosset, E. Lantz, S. Monneret, and H. Le Gall, "Image upconversion from the visible to the UV domain: application to dynamic UV microstereolithography," *Appl. Opt.* **40**(28), 4953–4957 (2001).
18. J. S. Dam, C. Pedersen, and P. Tidemand-Lichtenberg, "High-resolution two-dimensional image upconversion of incoherent light," *Opt. Lett.* **35**(22), 3796–3798 (2010).
19. J. Watson, P. Georges, T. Lépine, B. Alonzi, and A. Brun, "Imaging in diffuse media with ultrafast degenerate optical parametric amplification," *Opt. Lett.* **20**(3), 231–233 (1995).
20. R. W. Boyd, *Nonlinear Optics* (Academic Press, 2002).

21. N. P. Barnes and V. J. Corcoran, "Parametric generation processes: spectral bandwidth and acceptance angles," *Appl. Opt.* **15**(3), 696–699 (1976).
22. A. Shirakawa and T. Kobayashi, "Noncollinearly phase-matched femtosecond optical parametric amplification with a 2000  $\text{cm}^{-1}$  bandwidth," *Appl. Phys. Lett.* **72**(2), 147–149 (1998).
23. I. Jovanovic, B. J. Comaskey, and D. M. Pennington, "Angular effects and beam quality in optical parametric amplification," *J. Appl. Phys.* **90**(9), 4328–4337 (2001).
24. W. H. Louisell, A. Yariv, and A. E. Siegman, "Quantum fluctuations and noise in parametric processes. I," *Phys. Rev.* **124**(6), 1646–1654 (1961).
25. V. Krylov, J. Gallus, U. P. Wild, A. Kalintsev, and A. Rebane, "Femtosecond noncollinear and collinear parametric generation and amplification in BBO crystal," *Appl. Phys. B* **70**(2), 163–168 (2000).
26. R. Trebino, *Frequency-Resolved Optical Gating: The Measurement of Ultrashort Laser Pulses* (Kluwer Academic Publishers, 2002).
27. R. A. Andrews, "IR image parametric up-conversion," *IEEE J. Quantum Electron.* **6**(1), 68–80 (1970).

## 1. Optical-parametric-amplification imaging

The ultrahigh intensities available from ultrafast-laser technology allow access to a wide range of high-intensity phenomena and techniques. Whereas earlier laser systems required tightly focused beam spots in order to achieve sufficient intensities, recent advances in Ti:Sapphire regenerative amplifiers ("regens") allow high-intensity interactions of unfocused beams with relatively large diameters. Vastly improved stability in such amplifier systems also makes practical previously impractical highly nonlinear processes.

Optical parametric amplification (OPA) [1], in particular, which experiences gain that is an exponential of the pump-beam intensity, benefits greatly from these technological advances. OPA has long been used to nonlinear-optically amplify weak input signals [2], as well as to wavelength-convert them, usually from the infrared into the visible [3]. Unfortunately, due to its highly nonlinear nature, OPA is very sensitive to and severely limited by shot-to-shot jitter of the pump laser. Pulses that are too weak can yield no signal, and pulses that are too intense can yield outputs that saturate the detectors or, worse, damage the crystal. Such issues significantly complicate applications of OPA, and, as a result, OPA, perhaps more than any other optical process, benefits from the high intensity and, especially, the vastly improved shot-to-shot jitter of these laser systems.

Indeed, the use of OPA for imaging applications (see Fig. 1)—first demonstrated in 1968, when Midwinter amplified and frequency-shifted a one-dimensional infrared (IR) image to the visible [4]—should benefit greatly. OPA imaging involves imaging an object (or target) with amplification and perhaps also simultaneous wavelength conversion, spatial-frequency filtering, time-gating and phase conjugation. An imaging system then images or focuses the target onto a nonlinear medium, where an intense pump beam amplifies (and potentially wavelength shifts and time-gates) the target, and an additional imaging or focusing system transfers the target image from the OPA medium to a camera. Both monochromatic [5] and polychromatic [6] images have been amplified. When OPA is performed to amplify or frequency-shift an image, the interaction takes place between the input beams in the nonlinear medium, but different interaction planes can be used, depending on the imaging system used. The OPA crystal can be placed at an image plane, which is then re-imaged onto the detector [6,7]. Spatial frequency filtering in the real image domain is possible, but requires changing the crystal angle, which changes the spatial frequency transfer function of the system [8]. Placing the interaction plane at a focus causes the interaction to be in the Fourier plane of the image [9]. Using this interaction geometry should allow much greater control of the spatial frequency transfer function [10,11] by spatially shaping the pump beam. Another potentially useful property is that the difference-frequency generation (DFG) beam is the phase conjugate of the input image beam, and, with OPA, the phase conjugation occurs in the forward direction. As a result, OPA imaging can be performed without the use of imaging lenses [12–15]; if the same wavelength is used for the OPA and the DFG beams (that is, operating at degeneracy), an exact replica of the spatial distribution of the input, but with gain, appears the same distance after the nonlinear medium as the object before it.

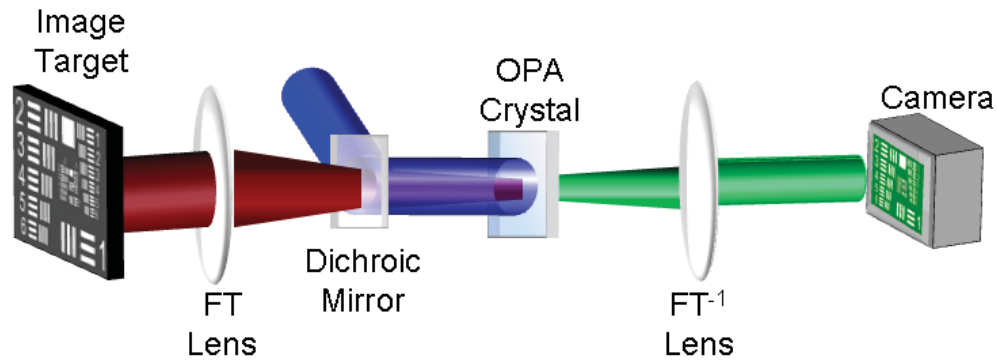


Fig. 1. A typical OPA imaging apparatus. An image target is illuminated with infrared light and transferred by a lens to a nonlinear crystal. A shorter-wavelength pump beam (shown in blue) overlaps the image-bearing signal at the nonlinear medium. The OPA process generates an intense replica of the image at a new (typically visible) wavelength. It simultaneously amplifies the infrared light (the amplified IR beam is not shown). The imaging or inverse Fourier-transforming ( $FT^{-1}$ ) lens then images or inverse Fourier transforms the field for detection at the camera.

The goal of such studies is the application of OPA for amplifying and wavelength-shifting a complex (i.e., interesting) image – one bearing a large spread of spatial frequencies in both the horizontal and vertical dimensions. To determine the complexity of an image, we utilize the two dimensional space-bandwidth product (SBP) [16], which is detailed in section 6. There has been success in wavelength-converted images using Sum Frequency Generation (SFG). The most complex image wavelength-converted using SFG in the real-image plane had a SBP of  $\sim 16,000$  [17]. Using SFG with the Fourier plane as the interaction plane, results of a SBP greater than 63,000 have been obtained [18]. Sum frequency generation has so far proven more successful than OPA in imaging complex objects, and these SBPs are significantly better than has been reported previously utilizing OPA as the nonlinear interaction. OPA, however, has the additional feature of amplification, and so developing this technique is desirable.

OPA imaging can be done with the crystal at an image plane of the object or at the Fourier plane of the object. With the crystal at the image plane, the best previously reported complexity contained 4 line-pairs/millimeter (lp/mm) in both the horizontal and vertical directions, and achieved amplification by an average factor of  $\sim 30$ , and had an SBP of  $\sim 6,000$  [6]. The most complex image to which OPA has been applied using the Fourier interaction plane yielded a high gain of  $>10^3$  [10], which is desirable, but with a resolution of only 1.25 lp/mm, and a SBP of only  $\sim 15$ . One major advantage to using OPA is the ability to achieve high gain. The highest gain ever reported using OPA imaging was in a ballistic-imaging experiment, where a gain of  $10^4$  was demonstrated [19], although this gain was across a one-dimensional image in which the detector position was scanned and the detected intensity mapped over many pulses, and had a one dimensional SBP of 1.

Here we extend this technology to the imaging of a more complex object and report two-dimensional OPA Fourier-plane imaging of spatial features from 1.1 to 10.1 line pairs/millimeter (lp/mm) in the vertical dimension and from 2.0 to 16.0 lp/mm in the horizontal dimension. We observe a gain of  $\sim 100$ , and, although our images were averaged over many shots, we used a single-shot geometry, capable of true single-shot OPA imaging. To our knowledge, this is the first Fourier-plane OPA imaging of more than a single spatial-frequency component of an image. The two-dimensional SBP for our Fourier-plane OPA imaging system was  $\sim 46,000$ .

## 2. Optimizing gain in OPA imaging

The main limitations on the achievable gain and image fidelity in OPA imaging involve phase-matching for the nonlinear interaction. The interacting beams must satisfy two conditions:

$$\omega_{PUMP} = \omega_{OPA} + \omega_{DFG} \quad (1a)$$

$$\vec{k}_{PUMP} = \vec{k}_{OPA} + \vec{k}_{DFG} \quad (1b)$$

where ‘*PUMP*’ refers to the pump (the shortest wavelength and most intense) beam, ‘*OPA*’ to the amplified beam at the input wavelength, which in our case is the infrared 930nm input, and ‘*DFG*’ to the wavelength-converted beam, which in our case was the visible 700nm beam. As is well-known for all nonlinear-optical processes, achieving phase-matching across the entire pulse bandwidth limits the crystal thickness and hence the efficiency [20]. The phase-matching process can be performed in several polarization configurations [20], where the phase-matching angle will depend on the polarization on the interacting beams. Here, we have used type-I phase-matching, where the pump beam is extraordinarily polarized, so that the OPA and DFG beams are both ordinarily polarized. Because the OPA and DFG beams are at different wavelengths, isolate either one or the other is simply a matter of filtering the desired beam.

The phase-matching process is not only limited by efficiency and spectral bandwidth consideration, but has a limited geometrical acceptance angle [21]. Equation (1b) deals with the wave-vectors during phase-matching. While the wave-vector lengths depend on the wavelengths, their directions depend on input angles of the interacting beams. In many OPA experiments, the change in the phase mismatch (the difference between the left hand and right hand sides of Eq. (1b)) as the wavelength is changed is minimized. This configuration is commonly referred to as non-collinear OPA, and can lead to amplification across a broad spectral range [22]. For imaging applications, it is more important to limit the change in phase mismatch as the angle of the interacting waves is changed [23]. As a result of the non-linear medium having a limited angular acceptance, the maximum spatial frequency that any OPA imaging system will be able to accept is limited by phase-matching considerations. Moreover, a somewhat uniform amplification across the entire image is desired in most OPA imaging applications. Therefore the gain profile, which is determined by the phase-matching, needs to be constant over the image. It is customary in OPA imaging to define a boundary for OPA imaging acceptance angles as the angular range over which the gain is always at least 50% of the maximum gain for ideal phase-matching [8].

The second limiting factor in an OPA imaging system is OPG [24,25], which involves phase-matching of beams *not* of interest. It is the generation of parametric super-fluorescence from noise background light due to the use of an input pump of high intensity. The background, also referred to as Optical Parametric Generation (OPG), degrades the amplified image and competes for available pump-beam energy. For uniaxial crystals, OPG is generated as a pair of concentric rings, each of longer wavelength than the pump, and the longer wavelength ring has a larger diameter. As a crystal’s phase-matching angle is changed, the diameters and central wavelengths of the OPG rings change, so that the phase-matching condition continues to be satisfied for the central wavelengths of each ring.

To minimize the problems presented by OPG, we chose crystal parameters so that the smaller OPG ring occurred at an angle outside the area of the image and used an aperture to separate the OPA image from the OPG background. We utilized a completely collinear beam geometry for the pump, OPA, and DFG beams, yielding less gain because the OPA process was not perfectly phase-matched. Nevertheless, we were still able to achieve over two orders of magnitude of amplification across the pulse spectrum. We also observed similar gain across a wide range of spatial features (that is, angles). We also used wavelength filters to separate the beams after the OPA crystal to isolate the OPA or DFG beam.

We measured the spectrum of the input beam and the amplified output beams. We found that, despite the phase-mismatch, the only noticeable spectral effect is a slight increase in bandwidth, shown in Fig. 2, which is an expected effect during OPA when either of the input beams is not well-collimated [22].

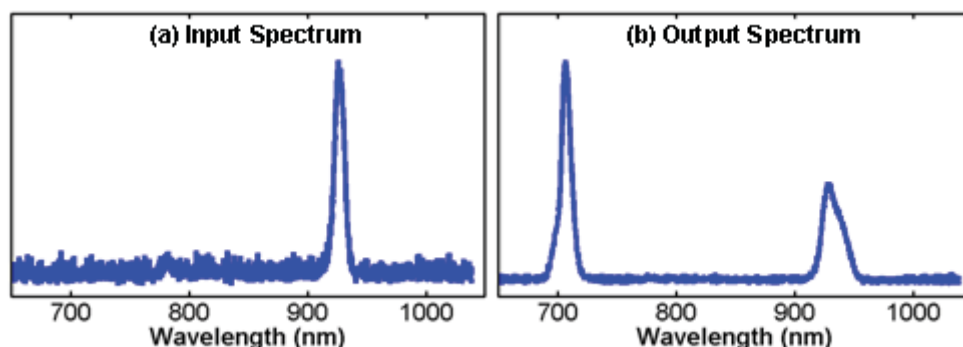


Fig. 2. (a) The input spectrum and (b) the two output spectra after the OPA are shown after background subtraction. The 930nm peak output spectrum is clearly broadened from the input spectrum. This result occurs during OPA when either of the input beams is not well-collimated. In OPA imaging, an image bearing signal cannot, by definition, be well-collimated and this broadening of the spectrum for the input wavelength will always occur. The output beam at the difference frequency is also clearly seen to have less bandwidth than the output OPA beam. This is also expected, as conservation of energy dictates that the bandwidth of the lower wavelength output beam during OPA will be narrower than the bandwidth of the longer wavelength beam.

### 3. Maximizing spatial resolution in OPA imaging

In addition to the above gain limitations, there are geometrical factors that limit the spatial resolution of OPA imaging systems. These include geometrical smearing due to the thickness of the nonlinear medium [26] and spatial imperfections of the pump beam, which are imprinted onto the amplified and wavelength-converted beams. In this section we explain how we maximized the spatial resolution of our imaging system by minimizing the distortions due to each of these effects.

The problem of geometrical smearing arises during OPA imaging when the image is placed in the real image plane. The pump beam and the input image-bearing beam cross at an angle. This leads to an amplified point generated at the leading edge of the crystal which differs in transverse position from amplified points generated later in the crystal. The amplified beam interacting with the image-bearing beam at different transverse positions in the crystal results in a single image point mapping to a range of transverse points in the resulting image, that is, an out-of-focus image.

In a real-image plane geometry, the way to limit geometrical smearing is to use an all-collinear beam geometry [27]. When the input and output beams are perfectly collinear, the transverse positions of the OPA beam do not vary across the crystal length, and geometrical smearing does not occur. However, while this holds perfectly for interactions of two plane waves, the definition of a complex and interesting image is a beam that contains a nonzero range of wave vectors. By its nature, then, an image cannot be perfectly collimated and so even use of a collinear geometry cannot completely eliminate geometrical smearing from OPA imaging when the amplification is performed in the real image plane geometry.

In the Fourier plane geometry, this is not the case. At the Fourier plane, the image information is contained in the angle of the light, not in its position. As a result, any displacement which does not cause a change in angle does not cause a distortion in this interaction geometry [27].

The effect of the pump beam must also be considered. It will play a different role for the two different geometrical configurations. In the real image plane geometry, the pump beam

acts as a physical aperture on the input image, and the image which can be recovered is limited by the size of the pump beam (or the lateral dimensions of the crystal). With the Fourier plane as the plane of interaction, the pump beams acts as a low-pass filter. Moreover, a Gaussian pump beam will cause there to be a non-uniform amplification across the spatial frequency spectrum. The highest spatial frequencies, which are furthest from the center in the Fourier plane, will be pumped by a less intense region of the Gaussian pump beam and will not experience as great amplification as the low spatial frequencies. The Fourier plane interaction necessarily includes imaging through a low-pass filter, and to recover a complex image requires having a pump beam of large enough lateral dimensions to allow the desired portion of the spatial frequency spectrum through this filter.

Utilizing a high-intensity amplified femtosecond pump pulse, we were able to use a much thinner nonlinear medium (1mm thick) than previous efforts. Previous demonstrations, conducted using picosecond pump pulses [6], required nonlinear media cm in length, or required multiple passes through the crystal [10]. Both of these configurations used a real-image plane geometry, with the result of significant geometrical smearing.

The quality of the pump beam spatial profile will also have an effect on the resolution achievable in OPA imaging systems. The highest resolution requires using a spatially smooth, collimated beam as a pump [27]. In previous demonstrations of OPA imaging, and in most other applications of OPA, the pump beam was focused in order to achieve the high pump intensities that OPAs require. Utilizing our high-power regen, we were able to spatially filter our beam to produce a clean spatial mode and pump our OPA with a well-collimated, unfocused, pump beam while still achieving peak intensities of over  $1\text{GW}/\text{cm}^2$ . This was done with a pump beam of 2mm diameter.

A second benefit of using a large-diameter pump beam is that it allows for overlap between a greater portion of the image-bearing beam with the pump beam, essentially making our low-pass filter have a higher cut-off spatial frequency than previous demonstrations, which allows more detail to be discerned in the final image.

#### **4. Experimental apparatus for OPA imaging in the Fourier plane**

In our experimental OPA imaging apparatus (Fig. 3), we amplified the output from a KM Labs kit oscillator with a Coherent Legend Elite Regenerative Amplifier to produce 40fs pulses centered at 800nm with pulse energies of 3mJ at a repetition rate of 1kHz. We performed second-harmonic generation in a 1mm BBO crystal to produce an e-polarized beam at 400nm with 1mJ per pulse, which was used as the pump in the OPA process.

While the beam from the regen was fairly unstructured to begin with, we built a spatial filter to remove the small amount of structure present in it as a result of the second harmonic process. It used a  $50\mu\text{m}$  wire die as the spatial-filter pinhole. The pinhole was contained in a 4Torr vacuum chamber to avoid nonlinear breakdown in air.

The output from our vacuum spatial filter was 0.5mJ per pulse and was down-collimated utilizing a positive and negative focal length lens pair so that the pump beam was collimated with a diameter of 2mm. The result of this spatial filter was to smooth the intensity profile, as shown in Fig. 4. The shot-to-shot pulse-energy jitter from the Coherent Legend Elite at the fundamental frequency was 0.56%. The shot-to-shot pulse-energy jitter at the second harmonic, which was used as the pump beam in our OPA after passing through the spatial filter was 0.94%. This clean spatial profile and stable shot-to-shot intensity allowed us to pump our OPA with a stable laser source.

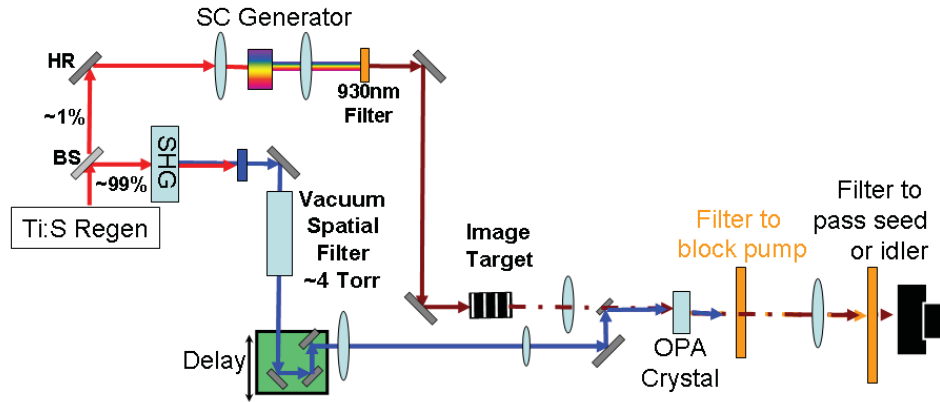


Fig. 3. OPA imaging experimental apparatus. The output from the amplifier was split into two beams. Most of the light was frequency-doubled to act as the OPA pump. The rest generated supercontinuum, part of which was used as the OPA input, which was passed through an image target. The pump was spatially filtered. The two beams were overlapped at a 1mm BBO crystal. A filter before the camera transmitted only the OPA beam (or the DFG beam), which was detected by the camera.

A small fraction of the 800nm pulse was focused through 3mm of fused silica to generate white-light supercontinuum. This continuum was then passed through an infrared band-pass filter, which transmitted 10nm of bandwidth centered at 930nm. This infrared wavelength range was selected for two reasons. First, the DFG beam through this process was centered at 700nm, demonstrating a shift from the infrared into the visible. Second, this infrared wavelength is detectable by the PixeLink PL-A741 CCD array we used to record the DFG beam, allowing measurement of the amplification of the infrared beam—a desirable situation in many practical applications of OPA imaging.

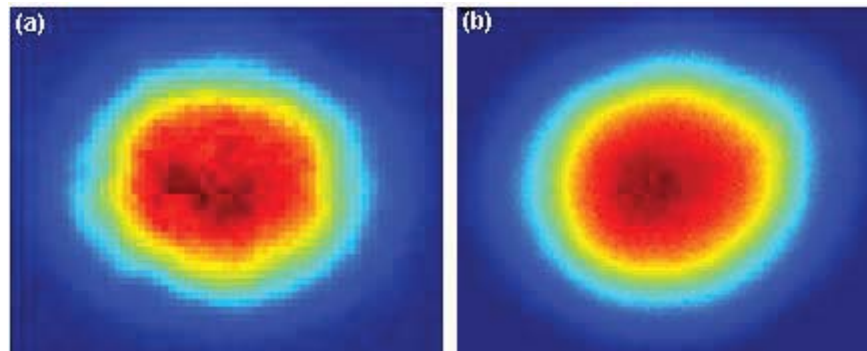


Fig. 4. Spatial profiles of the pump beam both (a) before and (b) after the spatial filter. The spatial profile before filtering displays several hot spots in the most intense regions of the beam. These hot spots are smoothed out by the filter. If they had been present in the beam, there would have been non-uniform amplification across the input image during the OPA process.

The image was generated by placing a transmitting USAF 1951 target in the infrared beam path. The output face of this target was placed one focal length before a 150mm-focal-length lens. At the focal plane, a 1mm-thick type-I BBO crystal, cut at a phase-matching angle of 29°, acted as the OPA medium. The 400nm pump beam was e-polarized, and interacted with an o-polarized seed beam. The generated OPA beam and DFG beam were both o-polarized as a result of this Type-I interaction. This crystal was mounted on a rotation stage so that it could be angle-tuned. Because the nonlinear medium was placed at the focus of this lens, the Fourier plane of the image became the interaction plane for the OPA imaging system. To perform the

inverse Fourier transform on the amplified OPA image or on wavelength-converted DFG beam, an achromatic 100mm second lens was placed its focal length after the nonlinear medium. The ratio of the focal lengths of these two lenses resulted in a de-magnified image at the camera.

Given the parameters of our experiment, we can determine the angular acceptance of the OPA imaging system. The angular acceptance defines the range of angles in the transverse plane which can be phase-matched with efficiency of at least 50% of the maximum efficiency [7]. Because of the symmetry of the USAF 1951 target, the expected resolution in the two lateral dimensions can be measured. For 1mm BBO in a type-I configuration, the half angular acceptance in the two transverse dimensions of  $\Delta\phi = \sim 13$  milliradians for the difference-frequency wavelength of 700nm. The crystal has a half-angular acceptance at the 930nm OPA signal wavelength of  $\Delta\phi = \sim 17$  milliradians. These angular ranges correspond to an expected maximum resolution of  $\sim 30 \text{ mm}^{-1}$  for both the signal and idler wavelengths.

## 5. Results and discussion

Our illuminated target, weak input image, OPA amplified image, and DFG wavelength-shifted image are shown in Fig. 5. This figure demonstrates both amplification of an IR image and amplification and wavelength down-conversion of a single image, both of the USAF 1951 test pattern. Both of these occur simultaneously, and band-pass filters at the appropriate wavelength were used to isolate either the OPA beam or the DFG beam. The circular edges which appear on the amplified image (Fig. 5(c)) and wavelength-shifted image (Fig. 5(d)) are a result of the illumination of our target test by a circular slice of supercontinuum, and not a result of the OPA interaction.

We consider first the OPA image at 930nm (Fig. 5(c)). To measure the amount of gain in the amplified infrared image, we deliberately decreased the supercontinuum beam intensity in order to generate a weak infrared seed (Fig. 5(b)). This decreased the input intensity to a level comparable with the noise floor of our camera. After the OPA crystal, the OPA amplified image (Fig. 5(c)) increased to an intensity just below the saturation level of the detector, implying an OPA image gain of  $\sim 100$  (the camera had only 8 bits of dynamic range). While features as fine as 57 lp/mm were resolvable in the input image, the Fourier plane OPA interaction acts as a low-pass filter for spatial frequencies in the image due to the resolution limitations discussed in Section 3. In our image, observable features spanned the range from 1.1 to 10.1 line pairs/millimeter (lp/mm) in the vertical dimension and span from 2.0 to 16.0 lp/mm in the horizontal dimension.

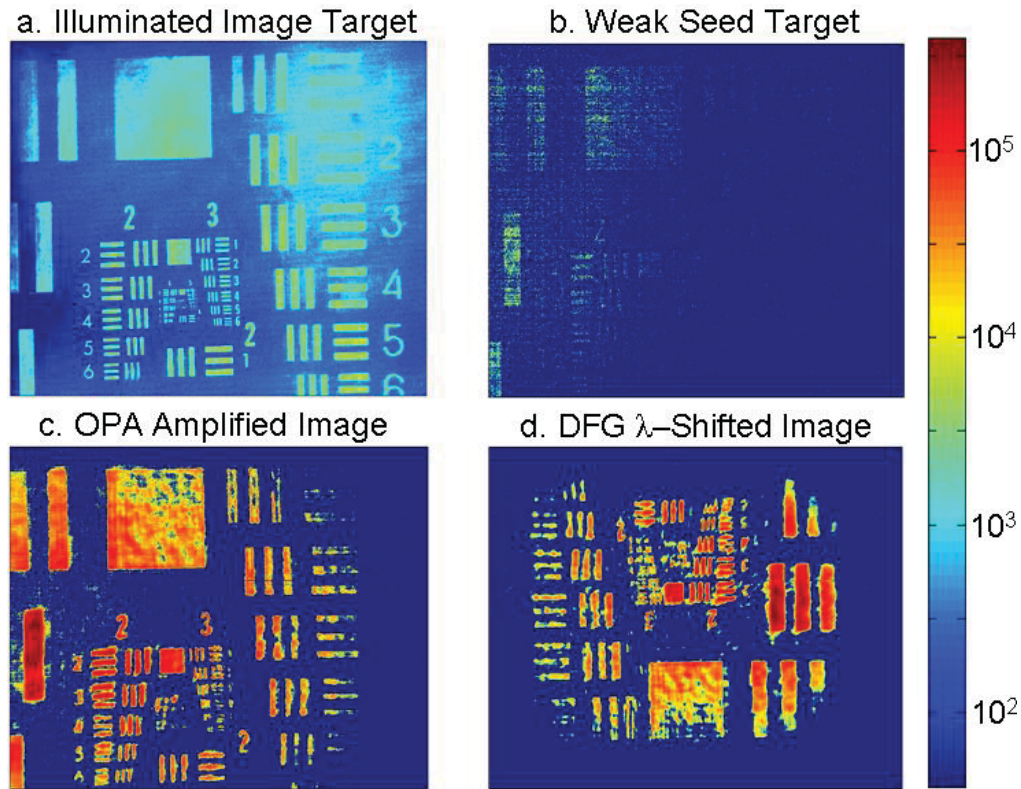


Fig. 5. (a) The USAF 1951 image target, containing resolvable spatial frequencies from 1.1 lp/mm in the vertical direction and 2 lp/mm in the horizontal direction to 57 lp/mm in both directions. (b) Decreasing the supercontinuum intensity so that the 930nm input image was close to the camera noise floor resulted in this barely measurable seed image. (c) Amplified OPA image at 930nm (i.e., not wavelength-shifted) with resolvable features as fine as 11.3 lp/mm. (d) The wavelength down-converted (frequency-upconverted) image recovered at 700nm with resolvable features as fine as 10.1 lp/mm, is observed to be demagnified and rotated 180° with respect to the input image and OPA image.

Figure 5(d) shows the DFG wavelength-converted image from the 930nm infrared input wavelength to a 700nm visible wavelength. The DFG image had resolvable features spanning the range from 1.1 to 10.1 lp/mm in both dimensions. This is a slight decrease in resolution compared with the amplified OPA image, which is due in part to the fact that this image has somewhat more noise than the amplified OPA beam. There is also angular demagnification that occurs during the conversion process [27], and so we observe a reduced image size. This angular demagnification occurs in all images where wavelength conversion shifts an image from a longer wavelength to a shorter one, and the amount of demagnification is the ratio of the input to output wavelength, which here will be a demagnification of  $930/700 = 1.3$ , which is the demagnification that we observe.

The detector face of the CCD camera we used was  $8.5\text{mm} \times 6.5\text{mm}$ , with pixels which are  $6.7\mu\text{m}$  square. The design of the USAF 1951 target is such that cameras are not able to simultaneously see the entire range of the largest features on the 1951 USAF target and also resolve the smallest features. Because the detector was rectangular and not square, we could not capture on it all of the largest horizontal and vertical features in the target simultaneously, while maintaining a magnification which would allow us to resolve the finest features in the target. We were able to capture vertical features as large as 1.1 lp/mm, but horizontal features from only 2 lp/mm. The performance of our OPA imaging system in the horizontal direction should not differ from the vertical direction, but, because we were limited by the size of the

detector, we could not compare the performances for the largest features on the target in the image.

## 6. The measured space-bandwidth product

The SBP [16] is a dimensionless measurement that nicely quantifies the complexity of the measured image. One way to construct this quantity is to take the product of the spatial extent of an image and the resolution (measured in spatial frequency) of that image. For a two-dimensional image, a SBP is computed for each transverse dimension, and the total SBP is the product of these two SBPs.

For the wavelength-unshifted OPA image, in the vertical dimension, we resolved in the amplified image features with a spatial resolution as fine as 10.1 lp/mm. The spatial extent of vertical features in our image spanned from the top edge of the group-0 features to the bottom edge of the group-2 features. This was a distance of  $\sim 8$ mm. The amplified image had a vertical SBP of  $\sim 150$ . In the horizontal dimension, the features spanned  $\sim 9$ mm with resolution of 16 lp/mm, so the horizontal SBP was  $\sim 300$ . The amplified image therefore had a two-dimensional SBP of  $\sim 45,000$ .

A similar calculation shows that, because of the slightly lower resolution achieved in the wavelength-shifted DFG image, the two-dimensional SBP for the wavelength-shifted image was  $\sim 30,000$ .

The largest two-dimensional SBP previously reported for OPA imaging in which the Fourier plane was the plane of interaction [10] we calculated to be  $\sim 15$ . The best previous measurement for OPA imaging using a real image plane as the plane of interaction [6] achieved a SBP of  $\sim 6,000$ .

Recording the space-bandwidth product requires measuring the spatial extent of the recovered image as well as the ability to resolve the finest features of the image. It is often the case, as it was in our case, that the camera is the main limitation of the ability to report a SBP, because using a magnification sufficient to resolve the fine features results in the largest features not fitting in the camera aperture. This can be overcome in a multi-shot geometry by using multiple  $FT^{-1}$  lenses with different magnifications to recover all the features, and can be overcome in a single-shot geometry by using a larger camera array or an array with smaller pixels so that large and fine features can be simultaneously recovered.

## 7. Conclusions

Taking advantage of recent advances in the engineering of high-power femtosecond regeneratively amplified laser system, we performed OPA amplification of an image utilizing the Fourier-transform plane as the plane of interaction. We OPA amplified a complex image both with and without wavelength-downconversion (frequency-upconversion), achieving two orders of magnitude of amplification across a large spread of spatial frequencies in the input image. This appears to be the most complex object ever imaged using OPA.